Journal of Power Sources 195 (2010) 567–573

Contents lists available at ScienceDirect

Journal of Power Sources

journal homepage: www.elsevier.com/locate/jpowsour

Cyclic deterioration and its improvement for Li-rich layered cathode material $Li[Ni_{0.17}Li_{0.2}Co_{0.07}Mn_{0.56}]O_2$

Atsushi Ito[a], Decheng Li[b,1], Yuichi Sato[b], Masazumi Arao[c], Manabu Watanabe[a], Masaharu Hatano[a], Hideaki Horie[a,d], Yasuhiko Ohsawa[a,*]

[a] Nissan Research Center, Nissan Motor Co., Ltd., 1, Natsushima-cho, Yokosuka, Kanagawa 237-8523, Japan
[b] Department of Material and Life Chemistry, Faculty of Engineering, Kanagawa University, 3-27-1, Rokkakubashi, Kanagawa-ku, Yokohama 221-8686, Japan
[c] Material Analysis Center, Research Department, NISSAN ARC, LTD., 1, Natsushima-cho, Yokosuka, Kanagawa 237-0061, Japan
[d] Research into Artifacts, Center for Engineering, the University of Tokyo, 5-1-5, Kashiwanoha, Kashiwa, Chiba 277-8568, Japan

ARTICLE INFO

Article history:
Received 1 April 2009
Received in revised form 29 July 2009
Accepted 30 July 2009
Available online 8 August 2009

Keywords:
Li-ion battery
Cathode material
$Li[Ni_{0.17}Li_{0.2}Co_{0.07}Mn_{0.56}]O_2$
Pre-cycling treatment
Cyclic deterioration
TEM

ABSTRACT

Transmission electron microscopy (TEM) studies were carried out to elucidate cyclic deterioration phenomena for Li-rich layered cathode material $Li[Ni_{0.17}Li_{0.2}Co_{0.07}Mn_{0.56}]O_2$. The results obtained show that the deterioration starts during the initial charge/discharge to higher potential over 4.5 V, and leads to the formation of micro-cracks at the crystal surface and the distortion of crystal periodicity. These two kinds of defects lead to further non-crystallization of the crystal surface and the emergence of a very small amount of another possible phase. Our stepwise pre-cycling treatment effectively depressed the formation of the former two kinds of defects, and could significantly improve cyclic durability. The observation of non-crystallization at the cathode crystal surface, which would diminish the battery performance, is consistent with our preliminary ac impedance results.

1. Introduction

In the nearly 20 years since Sony put Li-ion batteries on the market, extensive research has been carried out, and as a result, the specific energy has been raised more than double. Applications of Li-ion batteries to hybrid electric vehicles (HEVs) and electric vehicles (EVs) are very attractive and they recently have been tested worldwide to mitigate global warming. Future applications to such a large-sized device require larger capacity and better durability, and an increase in the capacity of the cathode material could be very effective in raising the specific energy of Li-ion batteries.

Recently, it has been reported that a solid solution system, Li_2MnO_3–$LiMO_2$ (M = Co and Ni, etc.), which can be considered as a Li-rich layered material, exhibits a high discharge capacity of more than 200 mAh g^{-1} when operated above 4.6 V. For example, charge–discharge properties have been reported for Li_2MnO_3–$LiNi_{1/2}Mn_{1/2}O_2$ [1,2], Li_2MnO_3–$LiCrO_2$ [3] and Li_2MnO_3–$Li[Ni_{1/3}Co_{1/3}Mn_{1/3}]O_2$ [4,5]. This kind of large capacity cathode material appears to still have cyclic durability problems for practical applications [6,7]. Wu and Manthiram tried to improve the durability by using a surface oxide coating [8].

In our previous paper [9], it was shown that the cyclic durability could be significantly improved though our stepwise pre-cycling treatment in which the quantity of Li^+ extracted and inserted during charge/discharge was increased gradually by controlling the upper potential limit above 4.5 V. The mechanism of this improvement to cyclic durability is still unclear. Therefore the present study examines cyclic deterioration phenomena for $Li[Ni_{0.17}Li_{0.2}Co_{0.07}Mn_{0.56}]O_2$ cathodes with and without our stepwise pre-cycling treatment by transmission electron microscopy (TEM).

2. Experimental

The preparation and characterization of $Li[Ni_{0.17}Li_{0.2}Co_{0.07}Mn_{0.56}]O_2$ using inductive-coupled plasma spectroscopy (I.C.P.) and XRD have been reported elsewhere [9]. The reference material Li_2MnO_3 was prepared using the standard solid state method from $LiOH{\cdot}H_2O$ and MnOOH for 10 h at 800 °C and then 12 h at 900 °C. Charge/discharge tests were performed using CR2032 coin-type cells including a cathode and a lithium metal anode. A pellet of the cathode mixture, which consisted of 20 mg of active material and 12 mg of Teflonized acetylene black (TAB-2) as the conducting

* Corresponding author. Tel.: +81 46 867 5367; fax: +81 46 865 5796.
E-mail address: y-oosawa@mail.nissan.co.jp (Y. Ohsawa).
[1] Present address: Light Industry Institute of Chemical Power Sources, Suzhou University, No. 688, Moye Road, Suzhou 215006, China.

0378-7753/$ – see front matter © 2009 Elsevier B.V. All rights reserved.
doi:10.1016/j.jpowsour.2009.07.052

binder, was pressed onto a stainless-steel mesh current collector of diameter 16 mm by applying a pressure of 1 ton cm^{-2}, and then dried at 130 °C for more than 4 h in a vacuum. The electrolyte was 1 M $LiPF_6$ solution of EC/DMC (1:2 by volume). The cells were assembled in a glove box filled with dry argon. Charge/discharge tests were performed at a constant current density of 0.2 mA cm^{-2} at room temperature in the potential range between 2.0 and 4.8 V. Our original stepwise pre-cycling treatment was carried out by increasing the upper potential limit by 0.1 V from 4.5 V every two cycles to 4.8 V, as reported elsewhere [9]. Ac impedance measurements were carried out for the coin-type cells including a cathode and a lithium metal anode at room temperature.

To investigate the features of the microstructure and crystal structure of the cathode samples obtained, we conducted TEM observations by means of a HITACHI H-9000UHR microscope with an acceleration voltage of 300 kV. The observations were made by taking bright-field (BF) images, high resolution transmission electron microscope (HRTEM) images, and selected area electron diffraction (SAED) patterns. Specimens for observations were powder samples supported on a copper micro-grid. To obtain charge/discharge cathode active material powders, coin-type cells were disassembled in the glove box, and the cathode samples were washed with dimethyl carbonate (DMC) several times, and then dried in a vacuum. Sample powders were scraped off of these cathodes.

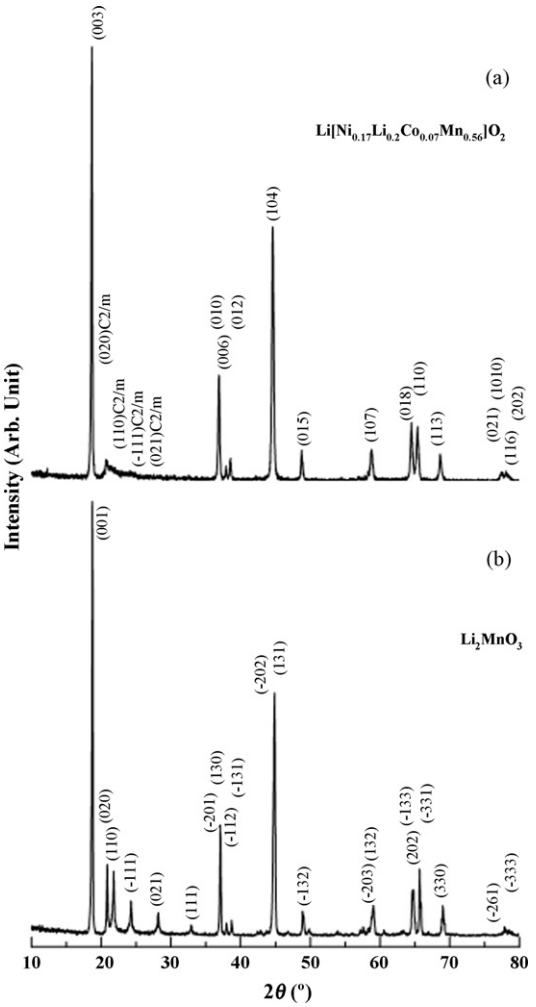

Fig. 1. XRD patterns of $Li[Ni_{0.17}Li_{0.2}Co_{0.07}Mn_{0.56}]O_2$ (a) and Li_2MnO_3 (b).

3. Results and discussion

3.1. Characterization of the as-prepared $Li[Ni_{0.17}Li_{0.2}Co_{0.07}Mn_{0.56}]O_2$

The elemental analysis results for the prepared $Li[Ni_{0.17}Li_{0.2}Co_{0.07}Mn_{0.56}]O_2$ were virtually the same as its nominal formula. Fig. 1a and b show XRD patterns of the prepared $Li[Ni_{0.17}Li_{0.2}Co_{0.07}Mn_{0.56}]O_2$ and Li_2MnO_3, respectively. In the XRD pattern of the $Li[Ni_{0.17}Li_{0.2}Co_{0.07}Mn_{0.56}]O_2$, a weak broad peak that appears to consist of broadened peaks of Li_2MnO_3 around 20–25° is observed at around 22°. Bréger et al. reported that this peak broadening is due to stacking faults [10]. Profile matching of XRD data of the prepared $Li[Ni_{0.17}Li_{0.2}Co_{0.07}Mn_{0.56}]O_2$ was possible with space group $R\bar{3}m$ or space group $C2/m$. The lattice parameters of this material with space group $R\bar{3}m$ were found to be $a_{hex.} = 2.853$ Å and $c_{hex.} = 14.22$ Å, and those with space group $C2/m$ were found to be $a_{mon.} = 4.954$ Å, $b_{mon.} = 8.543$ Å, $c_{mon.} = 5.036$ Å, and $\beta = 109°$.

Fig. 2 shows a typical low magnification BF image (Fig. 2a) and HRTEM image (Fig. 2b) of the as-prepared

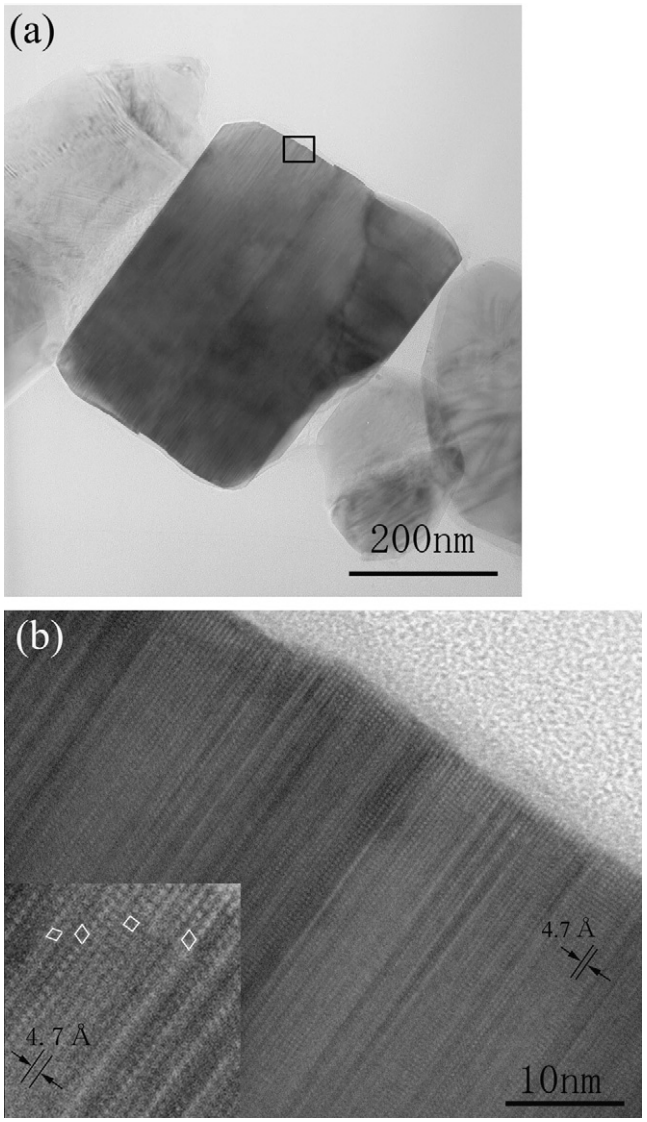

Fig. 2. Low magnification BF image (a) and HRTEM image (b) taken of the as-prepared $Li[Ni_{0.17}Li_{0.2}Co_{0.07}Mn_{0.56}]O_2$. The inset of (b) is a magnification of the HRTEM image.

$Li[Ni_{0.17}Li_{0.2}Co_{0.07}Mn_{0.56}]O_2$ sample. The HRTEM image (Fig. 2b) was taken from the surface of the particle in (Fig. 2a) designated by the square, and the electron incidence of these images was parallel to the $[\bar{1}\,1\,0]_{hex}$ zone axis. Note that the subscripts hex and mon represent the $LiNiO_2$-type ($R\bar{3}m$) and Li_2MnO_3-type ($C2/m$) structures, respectively. From Fig. 2a and other lower magnification BF images not shown here, the size of the primary particles ranged from 100 to 500 nm and the structure was polygonal. In the HRTEM image (Fig. 2b), there are bright- and dark-band contrasts with widths of a few nm, which are perpendicular to the $[0\,0\,1]_{hex}$ direction. In each band contrast, there is a fringe contrast with a space of 4.7 Å which corresponds to the inter-planar spacing of the $(0\,0\,3)_{hex}$ or the $(0\,0\,1)_{mon}$ plane. Furthermore, closer observation revealed that the fringe contrast consisted of a white dot array, which would have both of rectangular and parallelogram shapes, as shown in the inset of Fig. 2b. These shapes of white dot arrays seem to not be consistent with the $LiNiO_2$-type structure. This observation strongly suggests that the particle mainly consists of thin-plate-shaped regions with the Li_2MnO_3-type structure in three different orientations, with stacking faults between them, at

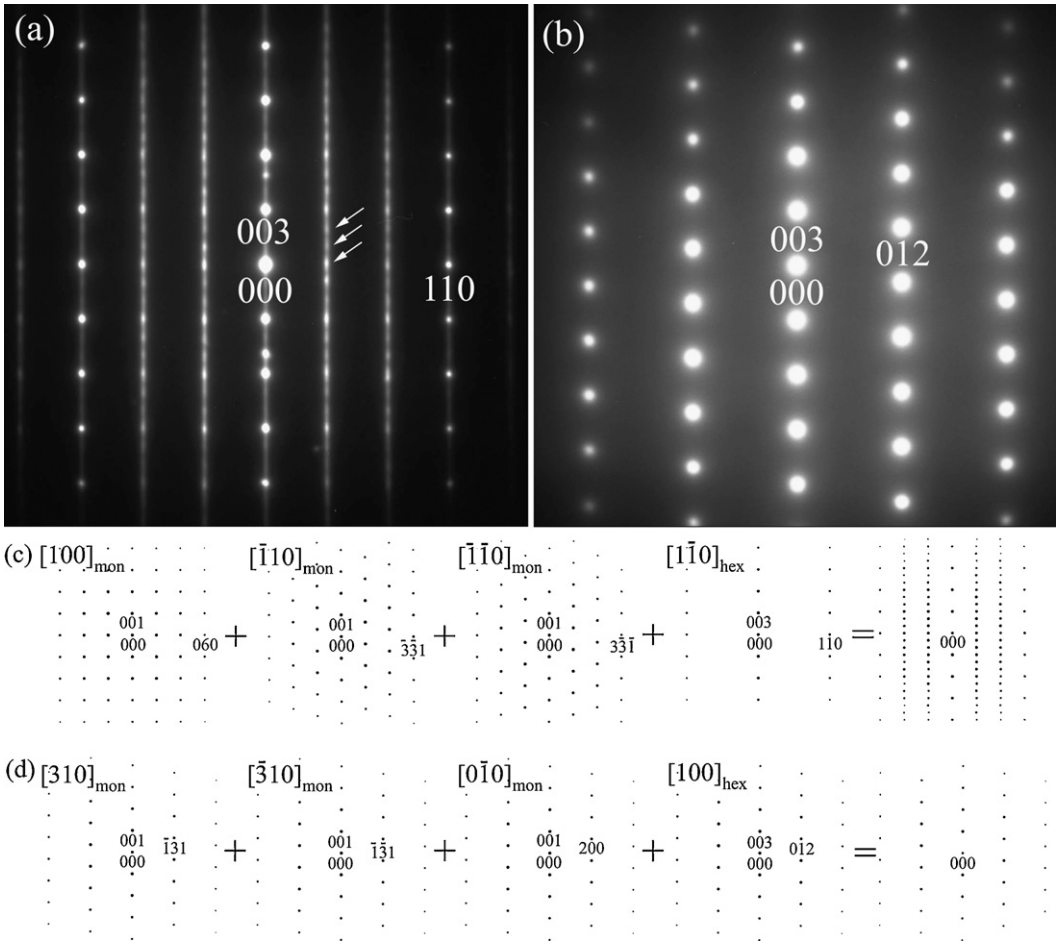

Fig. 3. SAED patterns taken of the as-prepared $Li[Ni_{0.17}Li_{0.2}Co_{0.07}Mn_{0.56}]O_2$ sample, (a), (b) and corresponding simulated schematic diagrams of the SAED patterns (c), (d). Electron incidences of (a) and (b) are parallel to the $[1\bar{1}0]_{hex}$ and the $[1\,0\,0]_{hex}$ zone axes, respectively.

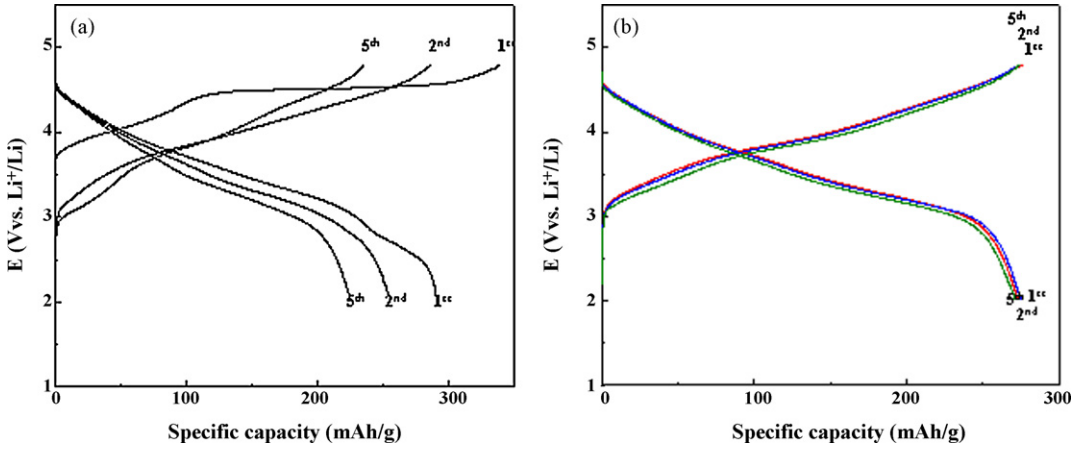

Fig. 4. Charge and discharge curves of the non-treated (a) and treated (b) $Li[Ni_{0.17}Li_{0.2}Co_{0.07}Mn_{0.56}]O_2$ electrodes with an increase in the cycle number.

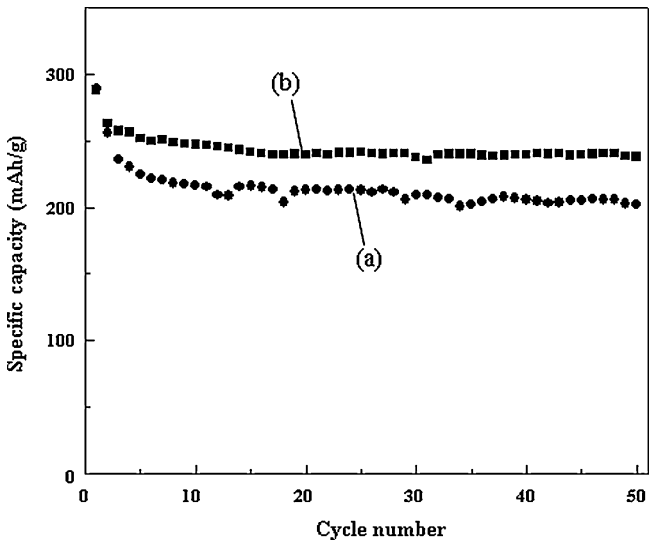

Fig. 5. Cyclic performance of the non-treated (a) and treated (b) $Li[Ni_{0.17}Li_{0.2}Co_{0.07}Mn_{0.56}]O_2$ electrodes.

least in this composition. This point was further examined using the SAED method.

Fig. 3a and b are the SAED patterns taken from the same particle used above. The electron incidence in Fig. 3a and b were respectively parallel to the $[1\,\bar{1}\,0]_{hex}$ and the $[1\,0\,0]_{hex}$ zone axes. For the sake of simplicity, the typical diffraction spots were indexed in terms of the $R\bar{3}m$ structure with hexagonal notation. One of the remarkable features of the pattern in Fig. 3a is that there are the forbidden spots at the $[1/3\ 1/3\ l]_{hex}$ positions, as pointed out by arrows, and these forbidden spots are slightly elongated in the $[0\,0\,1]_{hex}$ direction. Another feature is the existence of diffuse streaks through the forbidden spots. On the basis of the results of the HRTEM observations, this SAED pattern could be explained by the superposition of three SAED patterns of the Li_2MnO_3-type structure ($C2/m$) with different orientations, although the existence of pure $LiNiO_2$-type structure phase regions could not be eliminated since the SAED pattern of the $LiNiO_2$-type structure is superposed by those of the Li_2MnO_3-type structures. Fig. 3c shows the simulated $[1\,0\,0]_{mon}$, $[\bar{1}\,1\,0]_{mon}$, and $[\bar{1}\,\bar{1}\,0]_{mon}$ patterns with space group $C2/m$, together with the corresponding $[1\,\bar{1}\,0]_{hex}$ pattern with space group $R\bar{3}m$. The sum of these three (or four) patterns appears to reproduce the basic pattern in Fig. 3a. Furthermore, it is known that the streaks or elongated diffraction spots observed in the SAED are related to thin-plate-shaped regions or planar defects, such as stacking faults existing in the sample [11]. The SAED pattern of Fig. 3b is not inconsistent with our understanding of the SAED pattern of Fig. 3a since the simulated $[0\,\bar{1}\,0]_{mon}$, $[3\,1\,0]_{mon}$, $[\bar{3}\,1\,0]_{mon}$ and the corresponding $[1\,0\,0]_{hex}$ SAED patterns are identical, as shown in Fig. 3d. Our TEM results for the as-prepared $Li[Ni_{0.17}Li_{0.2}Co_{0.07}Mn_{0.56}]O_2$ sample are consistent with the recent report by Lei et al. about analytical electron microscopy of $Li[Ni_{0.2}Li_{0.2}Mn_{0.6}]O_2$ [12]. A more detailed TEM study is currently under way.

3.2. Charge/discharge properties

Charge/discharge curves for the as-prepared material in the potential range between 2.0 and 4.8 V are shown in Fig. 4a, and the initial charge and discharge capacities were 335 and 290 mAh g^{-1},

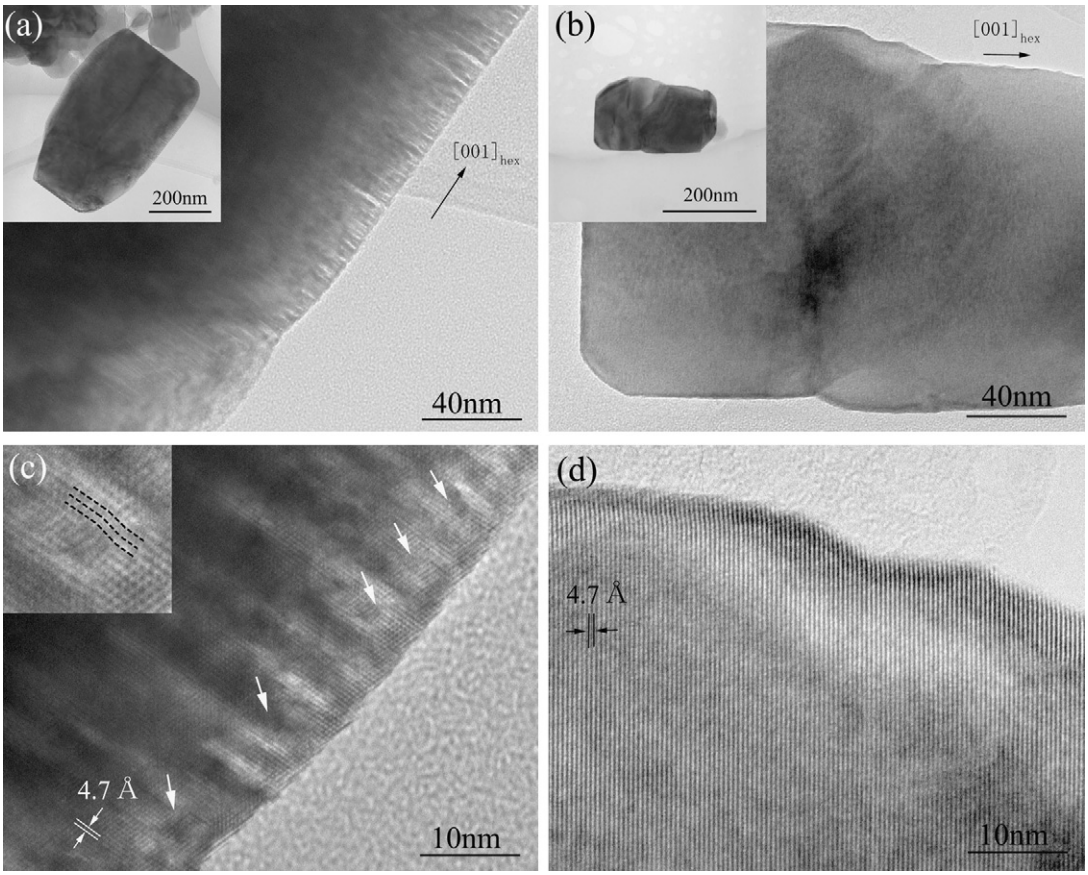

Fig. 6. BF and HRTEM images of the non-treated ((a) and (c)) and treated ((b) and (d)) $Li[Ni_{0.17}Li_{0.2}Co_{0.07}Mn_{0.56}]O_2$ after one charge/discharge cycle between 2.0 and 4.8 V. The BF images in (a) and (b) are magnifications of the surfaces of the particles shown in their insets. The inset of (c) shows a typical magnification of distorted parts in the particle shown by white arrows. The lattice fringe in the distorted part is traced by the dashed lines.

respectively. In this case, the discharge capacity rapidly decreased to 225 mAh g^{-1} of the 5th cycle. On the other hand, the cathode with the stepwise pre-cycling treatment showed more stable cyclic behavior, which is shown in Fig. 4b. The initial and the 5th discharge capacities were 275 and 273 mAh g^{-1}, respectively, and the discharge capacity virtually did not decrease.

Further cyclic durability tests were carried out for the cathodes both with and without the stepwise pre-cycling treatment, and the results are summarized in Fig. 5. The capacity retention without the treatment was only 68% after 50 cycles, and importantly the main part of this capacity fading occurred within the initial several cycles. On the other hand, the capacity retention of the cathode with the treatment was 90% after 50 cycles, and did not show a similar deterioration tendency. From these cyclic durability data, it is strongly suggested that the important causes of capacity deterioration would be brought about in the initial several charge/discharge cycles, especially the initial charging process, which is assumed to be accompanied by Li^+ extraction and O^{2-} oxidation [13], and that our stepwise pre-cycling treatment may proceed with this critical process gradually without causing severe damage to the cathode crystals. To clarify this point, TEM studies were carried out.

3.3. TEM analyses of the sample after charge/discharge cycle

TEM analyses were carried out on the cathode materials with and without the treatment, in order to investigate the microstructure from the BF and HRTEM images and to identify the crystal structure from the SAED patterns. We show the obtained results for the samples after the initial charge/discharge in Fig. 6, and those after 50 charge/discharge cycles in Fig. 7.

In the BF image taken from the cathode material without the treatment, Fig. 6a, many micro-cracks perpendicular to the c_{hex} axis are clearly observed at the surface of the particle. This kind of micro-cracks could be a serious cause of further cyclic deterioration. Similar micro-crack formation for Li-rich layered cathodes has been reported in Ref. [14] and the references cited therein. On the contrary, this kind of micro-crack formation was not observed in the samples with the treatment, as shown in Fig. 6b, and it appears that the microstructure did not change from the as-prepared state. HRTEM images of the particles without and with the treatment are shown in Fig. 6c and d, respectively. The lattice fringes with a spacing of 4.7 Å are observed in both images. The remarkable features are that the curved fringe contrasts are observed at some regions in Fig. 6c, as pointed out by white arrows, and these are not observed in Fig. 6d. These facts mean that the disorder in the crystal periodicity exists in the non-treated sample. It is believed that this kind of disorder in the crystal periodicity is also the result of deterioration in the initial charge/discharge, and could be a cause of further cyclic deterioration.

The results of TEM analyses for the samples after 50 charge/discharge cycles are shown in Fig. 7. As shown in Fig. 7a, amorphous regions without fringe contrast were observed at the surface of the particles without the treatment, together with the micro-cracks, which are not shown here. In other words, the deterioration phenomenon is surface non-crystallization of the particles. This surface non-crystallization, however, was not observed in the particles with the treatment, as shown in Fig. 7b.

Another experimental result indicating possible deterioration phenomena was obtained from the samples after 50 charge/discharge cycles. In Fig. 8a and b we show SAED patterns taken from the non-treated and the treated samples after 50 charge/discharge cycles, respectively, and the electron incidence is parallel to the $[1\,0\,0]_{hex}$ zone axis. In the SAED pattern taken from the non-treated sample, Fig. 8a, forbidden spots indicated by arrows A and B are observed in addition to the diffraction spots due to the $LiNiO_2$-type and/or the Li_2MnO_3-type structure. Among these

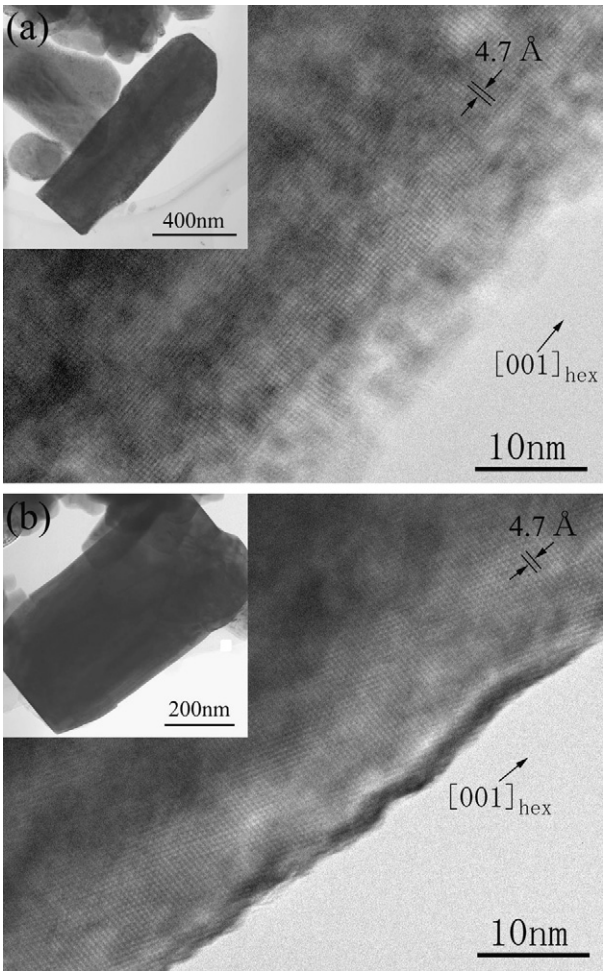

Fig. 7. HRTEM images of the non-treated (a) and treated (b) $Li[Ni_{0.17}Li_{0.2}Co_{0.07}Mn_{0.56}]O_2$ after 50 charge/discharge cycles between 2.0 and 4.8 V. The insets in (a) and (b) are the corresponding low magnification BF images and the HRTEM images were taken from the surfaces of the particles in the insets.

forbidden spots, the spots indicated by arrow A are also observed in SAED pattern in Fig. 8b taken from the treated sample. These forbidden spots are thought to be superlattice spots due to cation ordering or oxygen deficiency, although the origin of these spots is not clear. On the other hand, the forbidden spots indicated by arrows B are not observed in the SAED pattern from the treated sample. These weak spots suggest the possibility of the presence of another phase in the primary particle, which would affect the charge/discharge performance of the cathode material. However, further investigation of their crystal structure is needed.

3.4. Ac impedance measurements

The effect of the above mentioned cathode particle surface non-crystallization upon the charge/discharge properties was evaluated from preliminary ac impedance measurements for the coin-type cells including a cathode and a lithium metal anode. From this kind of surface degradation, the following internal resistance increases could be anticipated [15]. The first one whose phase minimum is located in a high-to-medium frequency range is due to the increase in resistance of the surface film of cathode particles. The physical meaning of the surface film resistance is complicated, although it is sometimes associated with Li^+ migration. In our case that may be associated with the contact resistance between the conducting additive and cathode particles. The second one whose phase mini-

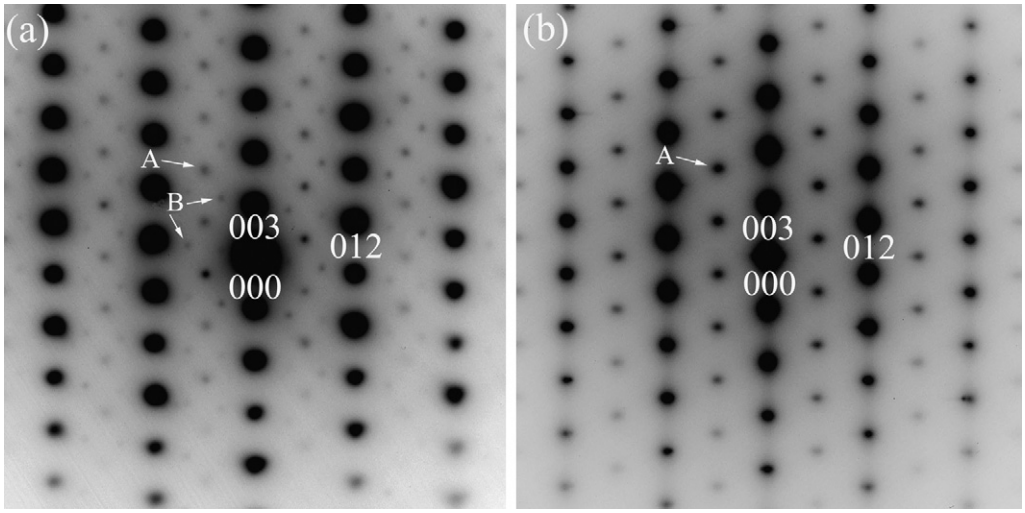

Fig. 8. SAED patterns taken from the non-treated (a) and treated (b) $Li[Ni_{0.17}Li_{0.2}Co_{0.07}Mn_{0.56}]O_2$ particles after the first charge/discharge cycle between 2.0 and 4.8 V. The electron incidence of both patterns is parallel to the $[1\,0\,0]_{hex}$ zone axis.

mum is located in a medium-to-low frequency range is due to the increase in charge-transfer resistance of cathode particles.

Fig. 9 shows the Bode plots for $Li/Li[Ni_{0.17}Li_{0.2}Co_{0.07}Mn_{0.56}]O_2$ cells at 50% SOC after the 2nd (a) and 10th cycle (b) without the pre-cycling treatment, and after the 1st (c) and 10th cycle (d) with the treatment. The corresponding two kinds of internal resistance increases were certainly observed for the $Li/Li[Ni_{0.17}Li_{0.2}Co_{0.07}Mn_{0.56}]O_2$ cell after the 10th cycle without the treatment in the corresponding frequency ranges, which is shown by (b) in Fig. 9, although a minor increase in the charge-transfer resistance was also observed for the $Li/Li[Ni_{0.17}Li_{0.2}Co_{0.07}Mn_{0.56}]O_2$ cell with the treatment, which is shown by (d) in Fig. 9. These two kinds of internal resistance increases upon charge/discharge cycling appear to be consistent with the surface non-crystallization, and definitely diminish the charge/discharge performance of a cell consisting of a $Li[Ni_{0.17}Li_{0.2}Co_{0.07}Mn_{0.56}]O_2$ cathode without the treatment.

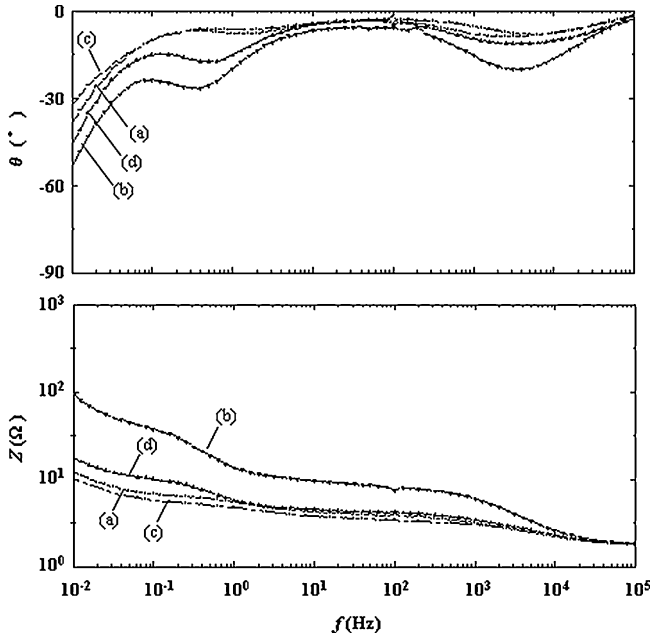

Fig. 9. The Bode plots of impedance data for $Li/Li[Ni_{0.17}Li_{0.2}Co_{0.07}Mn_{0.56}]O_2$ cells at 50% SOC (state of charge) after the 2nd (a) and 10th cycle (b) without the pre-cycling treatment, and after the 1st (c) and 10th cycle (d) with the pre-cycling treatment.

3.5. Physicochemical meaning of our pre-cycling treatment

Our treatment could activate inactive areas in the cathode crystals with only minimal structural change upon the initial charging above 4.5 V vs. $Li^{+/0}$. Regarding this initial charging, there are mainly two apparently controversial mechanisms proposed. The first proposed mechanism is summarized as follows [13]: Li^+ extraction is accompanied by oxygen ejection from the cathode crystals, which was observed as oxygen gas evolution by in situ differential electrochemical mass spectroscopy (DEMS), and transition metals in the surface region go into oxygen defects inside the crystals. This mechanism could partly explain the surface micro-cracks and distortion inside the crystals that were observed in this study. The other proposed mechanism is summarized as follows [16]: Li^+ extraction is not accompanied by oxygen ejection from the cathode crystals, which was experimentally supported by a smaller weight change of the cathode during the initial charge above 4.5 V. In this mechanism, π-bonding due to oxygen to metal donation is assumed to contribute to the charge compensation for Li^+ extraction, and thus keep the partially oxidized O^{2-} inside the cathode crystals. Even in the latter mechanism, partially oxidized O^{2-} in the surface region could oxidize electrolyte solvent, and lead to the formation of oxygen molecules, together with minimal structural degradation. From our data, both mechanisms appear to be possible, depending upon the material and charge/discharge conditions, and better conditions are successfully selected in our pre-cycling treatment. For practical applications of this sort of Li-rich layered cathode material, further research is under way in our group by considering these two mechanisms and the physicochemical meaning of our pre-cycling treatment.

4. Conclusions

Cyclic deterioration phenomena were studied for $Li[Ni_{0.17}Li_{0.2}Co_{0.07}Mn_{0.56}]O_2$ cathodes with and without our stepwise pre-cycling treatment. The results obtained show that the pre-cycling treatment effectively depressed the formation of micro-cracks at the surface of the crystals and the lattice distortion in the crystals during the initial charge to 4.8 V, which could be

causes of further cyclic deterioration: the non-crystallization of the crystal surface and the formation of a very small amount of another possible phase.

Acknowledgement

The authors acknowledge financial support from the Japanese New Energy and Industrial Technology Development Organization (NEDO).

References

[1] Z. Lu, L.Y. Beaulieu, R.A. Donaberger, C.L. Thomas, J.R. Dahn, J. Electrochem. Soc. 149 (2002) A778.
[2] S.-H. Kang, Y.K. Sun, K. Amine, Electrochem. Solid-State Lett. 6 (2003) A183.
[3] Z. Lu, J.R. Dahn, J. Electrochem. Soc. 149 (2002) A1454.
[4] M.M. Thackeray, S.-H. Kang, C.S. Johnson, J.T. Vaughey, R. Benedek, S.A. Hackney, J. Mater. Chem. 17 (2007) 3112.
[5] T.A. Arunkumar, Y. Wu, A. Manthiram, Chem. Mater. 19 (2007) 3067.
[6] Y.-S. Hong, Y.J. Park, K.S. Ryu, S.H. Chang, Solid State Ionics 176 (2005) 1035.
[7] S.-H. Kang, P. Kempgens, S. Greenbaum, A.J. Kropf, K. Amine, M.M. Thackeray, J. Mater. Chem. 17 (2007) 2069.
[8] Y. Wu, A. Manthiram, Electrochem. Solid-State Lett. 9 (2006) A221.
[9] A. Ito, D. Li, Y. Ohsawa, Y. Sato, J. Power Sources 183 (2008) 344.
[10] J. Bréger, M. Jiang, N. Dupré, Y.S. Meng, Y. Shao-Horn, G. Ceder, C.P. Grey, J. Solid State Chem. 178 (2005) 2575.
[11] P.B. Hirsch, A. Howie, R. Nicholson, D.W. Pashley, M.J. Whelan, Electron Microscopy of Thin Crystals, Butterworths, 1965.
[12] C.H. Lei, J. Bareño, J.G. Wen, I. Petrov, S.-H. Kang, D.P. Abraham, J. Power Sources 178 (2008) 422.
[13] A.R. Armstrong, M. Holzapfel, P. Novák, C.S. Johnson, S.-H. Kang, M.M. Thackeray, P.G. Bruce, J. Am. Chem. Soc. 128 (2006) 8694.
[14] N. Kumagai, J.-M. Kim, S. Tsuruta, Y. Kodama, K. Ui, Electrochim. Acta 53 (2008) 5287.
[15] K.M. Shaju, G.V.S. Rao, B.V.R. Chowdari, J. Electrochem. Soc. 150 (2003) A1.
[16] Y.-S. Hong, Y.J. Park, K.S. Ryu, S.H. Chang, M.G. Kim, J. Mater. Chem. 14 (2004) 1424.